

# SAMP-1: A Semi-Analytical Model for the Simulation of Polymers

S. Kolling <sup>a</sup>, A. Haufe <sup>b</sup>, M. Feucht <sup>a</sup> & P.A. Du Bois <sup>c</sup>

<sup>a</sup> DaimlerChrysler AG, EP/SPB, HPC X411, 71059 Sindelfingen, Germany

<sup>b</sup> DYNAmore GmbH, Industriestr. 2, 70565 Stuttgart, Germany

<sup>c</sup> Consulting Engineer, Freiligrathstr. 6, 63071 Offenbach, Germany

## Correspondence:

Dr. Stefan Kolling  
DaimlerChrysler AG  
HPC X411  
D-71059 Sindelfingen  
Germany

Tel: +49-(0)7031 - 9082829  
Fax: +49-(0) 7031 - 9078837  
e-mail: stefan.kolling@daimlerchrysler.com

## 1 Introduction

The numerical simulation of structural parts made from plastics is becoming increasingly important nowadays. The fact that almost any structural requirement can be combined in a lightweight, durable and cost effective structure is the driving force behind its widespread application. More and more structural relevant parts are being constructed and manufactured from plastics. This on the other hand drives the demand for reliable and robust methods to design these parts and to predict their structural behaviour. The key ingredients that need to be available are verified, calibrated and validated constitutive models for any family of plastic material. This holds not only true for crashworthiness applications but for any other application field.

Under high velocity impact loading, thermoplastic components undergo large plastic deformations and will most likely fail. Consequently, the unloading behaviour is irrelevant and thermoplastics can be modelled with a sufficiently good approximation as pseudo-metallic elastic-plastic bodies. This is, however, not always the case – even in crashworthiness applications. Nowadays important applications in crash simulation that demand a more accurate modelling of thermoplastics are simulation problems in pedestrian protection, e.g. head and leg impact (see [6], [10], [11], [12]) and passenger protection. Although highly sophisticated material laws are available in commercial finite element programs, there are still open questions, especially in the aforementioned field of application. In this pa-

per, the main focus is set to the explicit solver of LS-DYNA (see [1], [2]) but clearly with some effort all results are transferable to other solvers. In the following, an overview on classical models for polymers which are used for crash simulations nowadays is given. From a practical point of view, the usually applied constitutive model is material no. 24 (MAT\_PIECEWISE\_LINEAR\_PLASTICITY), a classical elastic-plastic model based on the vonMises criteria. It should be strongly emphasised though, that thermoplastics are not incompressible during plastic flow. This leads to the conclusion that material laws based on the vonMises criterion are not suitable in general (compare [13], [14], [15] & [22]). Therefore, a new material model which has been implemented into LS-DYNA as a user defined constitutive model will be the main focus of the present contribution.

Based on experimental work, important phenomena like necking, strain rate dependency, unloading behaviour and damage can be identified for certain polymer materials. A constitutive model including all the experimental findings and phenomena is derived. In particular, different behaviour in compression, tension and shear, as well as a strong strain rate dependent failure need to be addressed. Moreover, strain dependent damaging and damage induced erosion are both noticeable properties that need to be included in a constitutive model. The necessity of a pressure dependent formulation was shown in [4] where a classical Drucker-Prager (see [8], [9]) formulation was used to simulate a simple three point bending test. But for the aforementioned application in pedestrian protection, i.e. leg impact, this simple model is not accurate enough. In such load cases the bumper fascia will typically undergo only small straining and the deflection will be largely elastic while the unloading phase is of fundamental importance for the determination of the bending angle in the leg-form. Here, the degradation of elastic parameters (damaging) and the visco-elastic response is of uttermost importance. These key properties will be exemplified in the following discussion.

If the true stress-true strain curve of a typical thermoplastic is considered, it is well known that a reversal of curvature indicating a softening phase is often followed by a hardening phase. Thus a typical bone shaped specimen in a tension test shows necking at very low strains corresponding to the initial softening of the material. The subsequent hardening, however, results in a stabilization of the necked area and a redistribution of the plastic strains over the entire specimen. Unlike metals, the primary energy-absorbing potential of the thermoplastic resides at plastic strains beyond the necking value.

This type of physical response can be modelled perfectly using standard elastic-plastic material laws although the plastic deformation of thermoplastics is not isochoric as mentioned above. A further effect which has to be considered, though, is the unloading behaviour of the material. Usually, this is addressed by a damage parameter. It will be shown, that an approach where a scalar damage value is tabulated against equivalent plastic strains is a simple yet effective means to model such behaviour.

All effects associated with thermoplastics can be approximately considered in simple material models: Necking by an elastic-plastic law, unloading behaviour by a damage model; pressure dependent behaviour e.g. by standard Drucker-Prager model (see [4]). A new constitutive model, termed as SAMP-1 (**S**emi-**A**nalytical **M**odel for **P**olymers with  $C^1$ -differentiable yield surface, see [3], [5]) is derived in the following. The main focus of the present project is to include all relevant experimentally observed effects in one model.

## 2 Material law formulation

### 2.1 Yield surface formulation for plastics

Elastic-plastic material laws have been developed historically for the description of metallic materials based on crystal plasticity. The most commonly used example of this type implemented in LS-DYNA is MAT\_PIECEWISE\_LINEAR\_PLASTICITY which is based on the vonMises criteria. The same approach can be applied to some degree to the simulation of thermoplastics. However, it should be noted that very important differences exist between metals and thermoplastics. In particular, plastics have no constant modulus of elasticity and the different yield criteria under tension and compression preclude the use of a vonMises type of yield surface. Furthermore, the hardening of thermoplastics is anisotropic and the plastic deformation does not happen at constant volume. This lack of plastic incompressibility requires a flow rule allowing for permanent volumetric deformation. None of these effects can be considered in a classical (metallic) elastic-plastic material law. For an overview, some materials considering plasticity limited to materials with isotropic behaviour are listed in Table 1.

Law	Keyword	Hardening	Rate effect
3	MAT_PLASTIC_KINEMATIC	Linear	CS
12	MAT_ISOTROPIC_ELASTIC_PLASTIC	Linear	CS
15	MAT_JOHNSON_COOK	Power law	JC
18	MAT_POWER_LAW_PLASTICITY	Power law	CS
19	MAT_STRAIN_RATE_DEPENDENT_PLASTICITY	Linear	load curves
24	MAT_PIECEWISE_LINEAR_PLASTICITY	Load curve	CS, tabulated
81	MAT_PLASTICITY_WITH_DAMAGE	Load curve	CS, tabulated
89	MAT_PLASTICITY_POLYMER	Load curve	CS, tabulated
98	MAT_SIMPLIFIED_JOHNSON_COOK	Power law	JC
105	MAT_DAMAGE_2 (VISCO-PLASTIC)	Power law	Perzyna
112	MAT_FINITE_ELASTIC_STRAIN_PLASTICITY	Load curve	CS, tabulated
123	MAT_MODIFIED_PIECEWISE_LINEAR_PLASTICITY	Load curve	Load curve

Table 1: Overview of plastic materials in LS-DYNA.

### 2.1.1 Choice of a yield surface formulation

All plastics are to some degree anisotropic. The anisotropic characteristic can be due to fibre reinforcement, to the moulding process or it can be load induced in which case the material is at least initially isotropic. Therefore a quadratic form in the stress tensor is often used to describe the yield surface (see Bardenheier [7]). We restrict the scope of this work to isotropic formulations. However, the choice of this yield surface was made in view of later anisotropic generalisations. In the isotropic case the most general quadratic yield surface can be written as

$$f = \boldsymbol{\sigma}^T \mathbf{F} \boldsymbol{\sigma} + \mathbf{B} \boldsymbol{\sigma} + F_0 \leq 0, \quad (1)$$

where

$$\boldsymbol{\sigma} = \begin{pmatrix} \sigma_{xx} \\ \sigma_{yy} \\ \sigma_{zz} \\ \sigma_{xy} \\ \sigma_{yz} \\ \sigma_{zx} \end{pmatrix} \quad \mathbf{F} = \begin{pmatrix} F_{11} & F_{12} & F_{12} & 0 & 0 & 0 \\ F_{12} & F_{11} & F_{12} & 0 & 0 & 0 \\ F_{12} & F_{12} & F_{11} & 0 & 0 & 0 \\ 0 & 0 & 0 & F_{44} & 0 & 0 \\ 0 & 0 & 0 & 0 & F_{44} & 0 \\ 0 & 0 & 0 & 0 & 0 & F_{44} \end{pmatrix} \quad \mathbf{B} = \begin{pmatrix} F_1 & 0 & 0 & 0 & 0 & 0 \\ 0 & F_1 & 0 & 0 & 0 & 0 \\ 0 & 0 & F_1 & 0 & 0 & 0 \\ 0 & 0 & 0 & 0 & 0 & 0 \\ 0 & 0 & 0 & 0 & 0 & 0 \\ 0 & 0 & 0 & 0 & 0 & 0 \end{pmatrix}. \quad (2)$$

Some restrictions apply to the choice of the coefficients (see [21]). The existence of a stress-free state and the equivalence of pure shear and biaxial tension/compression require respectively

$$F_0 \leq 0 \quad \text{and} \quad F_{44} = 2(F_{11} - F_{12}) \quad (3)$$

Although four independent coefficients remain in the expression for the isotropic yield surface at this point, the yield condition is not affected if all coefficients are multiplied by a constant. Consequently only three coefficients can be freely chosen and three experiments under different states of stress can be fitted by this formulation. Without loss of generality the expression for the yield surface can be reformulated in terms of the first two stress invariants: pressure and vonMises stress.

$$p = -\frac{\sigma_{xx} + \sigma_{yy} + \sigma_{zz}}{3} \quad (4)$$

$$\sigma_{vm} = \sqrt{\frac{3}{2} \left( (\sigma_{xx} + p)^2 + (\sigma_{yy} + p)^2 + (\sigma_{zz} + p)^2 + 2\sigma_{xy}^2 + 2\sigma_{yz}^2 + 2\sigma_{zx}^2 \right)}$$

The expression for the yield surface then becomes

$$f = \sigma_{vm}^2 - A_0 - A_1 p - A_2 p^2 \leq 0 \quad (5)$$

and identification of the coefficients leads to

$$A_0 = -F_0, \quad A_1 = 3F_1 \quad \text{and} \quad A_2 = 9(1 - F_{11}) \quad (6)$$

or equivalently

$$F_0 = -A_0, \quad F_1 = \frac{A_1}{3}, \quad F_{11} = 1 - \frac{A_2}{9}, \quad F_{44} = 3 \quad \text{and} \quad F_{12} = F_{11} - \frac{F_{44}}{2} = -\left(\frac{1}{2} + \frac{A_2}{9}\right). \quad (7)$$

Since there is no loss of generality, the simpler formulation in invariants is adopted from this point on. In principle the coefficients of the yield surface can now be determined from the aforementioned three experiments. Typically one would perform uniaxial tension, uniaxial compression and simple shear tests as depicted in Fig 1.

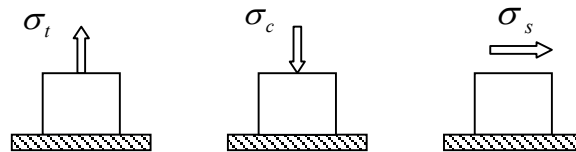


Figure 1: Recommended tests for material data in SAMP-1

This allows computation of the coefficients as functions of the test results:

$$\left. \begin{array}{l} 3\sigma_s^2 = A_0 \\ \sigma_t^2 = 3\sigma_s^2 - A_1 \frac{\sigma_t}{3} + A_2 \frac{\sigma_t^2}{9} \\ \sigma_c^2 = 3\sigma_s^2 + A_1 \frac{\sigma_c}{3} + A_2 \frac{\sigma_c^2}{9} \end{array} \right\} \Rightarrow \left\{ \begin{array}{l} A_0 = 3\sigma_s^2 \\ A_1 = 9\sigma_s^2 \left( \frac{\sigma_c - \sigma_t}{\sigma_c \sigma_t} \right) \\ A_2 = 9 \left( \frac{\sigma_c \sigma_t - 3\sigma_s^2}{\sigma_c \sigma_t} \right) \end{array} \right. \quad (8)$$

Alternatively one may also compute the coefficients relating the formulation in stress space:

$$\left. \begin{array}{l} F_0 + F_1 \sigma_t + F_{11} \sigma_t^2 = 0 \\ F_0 - F_1 \sigma_c + F_{11} \sigma_c^2 = 0 \\ F_0 + F_{44} \sigma_s^2 = 0 \end{array} \right\} \Rightarrow \left\{ \begin{array}{l} F_1 = F_0 \left( \frac{1}{\sigma_c} - \frac{1}{\sigma_t} \right) \\ F_{11} = -\frac{F_0}{\sigma_t \sigma_c} \\ F_{44} = -\frac{F_0}{\sigma_s^2} \end{array} \right. \quad (9)$$

Both are easily seen to be equivalent.

### 2.1.2 Conditions for convexity of the yield surface

#### 2.1.2.1 Introductory remarks

Usually the yield surface is required to be convex, i.e.

$$\left. \begin{array}{l} f(\boldsymbol{\sigma}_1) \leq 0 \\ f(\boldsymbol{\sigma}_2) \leq 0 \\ 0 \leq \alpha \leq 1 \end{array} \right\} \Rightarrow f(\alpha \boldsymbol{\sigma}_1 + (1-\alpha) \boldsymbol{\sigma}_2) \leq 0 \quad (10)$$

The second derivative of  $f$  is computed as

$$f = \boldsymbol{\sigma}^T \mathbf{F} \boldsymbol{\sigma} + \mathbf{B} \boldsymbol{\sigma} + F_0 \rightarrow \frac{\partial^2 f}{\partial \boldsymbol{\sigma}^2} = 2\mathbf{F} \quad (11)$$

A sufficient condition for convexity in 6D stress space is then that the matrix  $\mathbf{F}$  should be positive semidefinite. This means all eigenvalues of  $\mathbf{F}$  should be positive or zero. The conditions for convexity will now be examined in physical terms for two cases: plane stress and general 3D.

#### 2.1.2.2 The plane stress case

In the plane stress case the yield condition reduces to:

$$f = \boldsymbol{\sigma}^T \mathbf{F} \boldsymbol{\sigma} + \mathbf{B} \boldsymbol{\sigma} + F_0 \quad (12)$$

where

$$\boldsymbol{\sigma} = \begin{pmatrix} \sigma_{xx} \\ \sigma_{yy} \\ \sigma_{xy} \end{pmatrix} \quad \mathbf{F} = \begin{pmatrix} F_{11} & F_{12} & 0 \\ F_{12} & F_{11} & 0 \\ 0 & 0 & F_{44} \end{pmatrix} \quad \mathbf{B} = \begin{pmatrix} F_1 & 0 & 0 \\ 0 & F_1 & 0 \\ 0 & 0 & 0 \end{pmatrix}. \quad (13)$$

Furthermore convexity requires the eigenvalues of  $\mathbf{F}$  to be non-negative:

$$\left. \begin{array}{l} F_{11} + F_{12} \geq 0 \\ F_{11} - F_{12} \geq 0 \\ F_{44} \geq 0 \end{array} \right\} \Rightarrow \begin{cases} 4\sigma_s^2 \geq \sigma_t \sigma_c \\ -F_0 \geq 0 \end{cases} \quad (14)$$

Representation of the yield surface in the principal stress space allows a geometrical interpretation, see Figure 2. Clearly as long as

$$\sigma_s > \frac{\sqrt{\sigma_t \sigma_c}}{2}, \quad (15)$$

the yield surface is elliptic and thus convex. In the case of

$$\sigma_s = \frac{\sqrt{\sigma_t \sigma_c}}{2} \quad (16)$$

the yield surface degenerates into two straight lines. And for

$$\sigma_s < \frac{\sqrt{\sigma_t \sigma_c}}{2} \tag{17}$$

the yield surface becomes hyperbolic and convexity is lost. It can be seen that a non-convex yield surface is physically not plausible under plane stress conditions since no yielding will occur under biaxial loading.

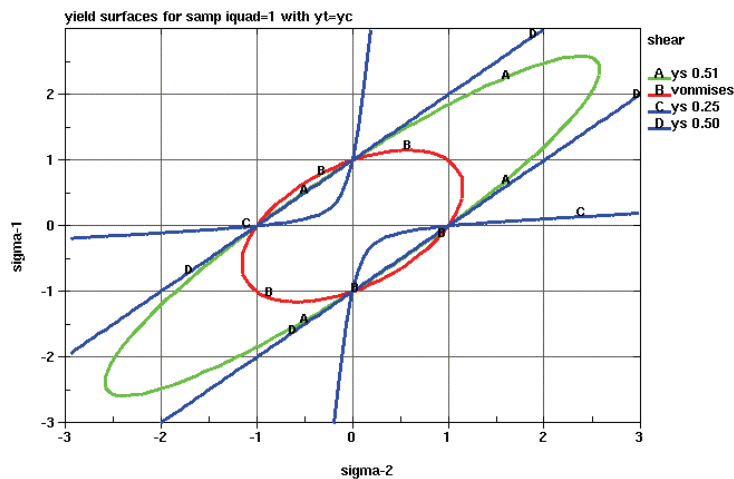


Figure 2: Representation of the yield surface in the principal stress plane

In the invariant plane the convexity condition for the plane stress case is easily seen to lead to the following condition:

$$\sigma_s \geq \frac{\sqrt{\sigma_t \sigma_c}}{2''} \Rightarrow A_2 \leq \frac{9}{4} \tag{18}$$

Thus, positive values of  $A_2$  are allowed and the yield curve can actually show a limited positive curvature.

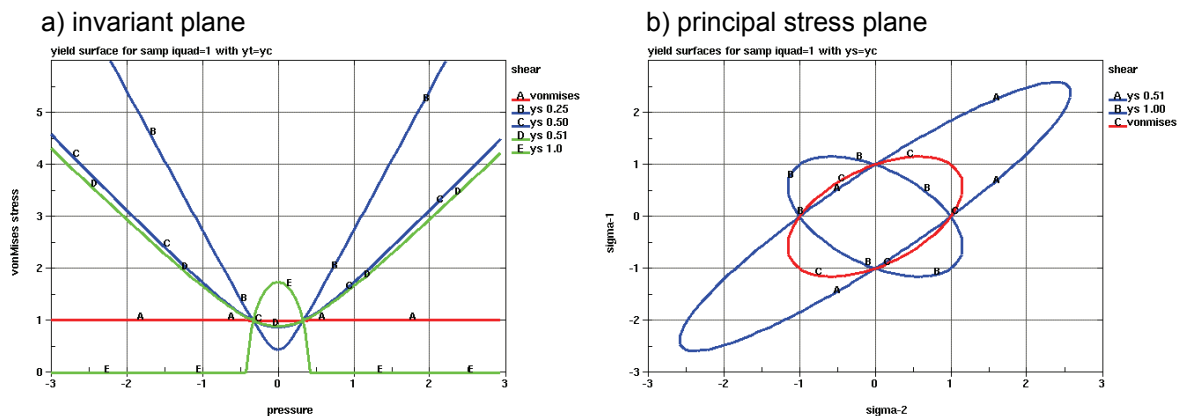


Figure 3: Convexity of the yield surface

In Figure 3a, it is shown that convex yield surfaces in principal stress space are guaranteed as long as the yield curve has a finite intersection with the biaxial line:

$$\left. \begin{aligned} \sigma_{vm}^2 - A_0 - A_1 p - A_2 p^2 = 0 \\ \sigma_{vm} = \pm \frac{3p}{2} \end{aligned} \right\} \frac{9p^2}{4} - A_0 - A_1 p - A_2 p^2 = 0. \quad (19)$$

This last equation will have a real finite solution for the pressure  $p$  iff

$$A_1^2 + 4A_0 \left( \frac{9}{4} - A_2 \right) \geq 0 \Rightarrow \sigma_s \geq \frac{\sqrt{\sigma_t \sigma_c}}{2}, \quad (20)$$

which is equivalent to requiring a convex yield surface in principal stress space. Examples of convex yield surfaces are shown in Figure 3b. Some corresponding remarks are summarized in Table 2.

$\frac{\sigma_s}{\sqrt{\sigma_t \sigma_c}}$	$A_2$	Remarks
1	-18	$\nu_p < 0$
0.707	-4.5	$\nu_p = 0$
0.57735	0	vonMises $\nu_p = 0.5$
0.5	2.25	No biaxial yield
0	9	No shear strength

Table 2: Remarks on yield surface parameters

### 2.1.2.3 The 3D case

In the full 3D case, the convexity condition is generally more stringent. Again we require the eigenvalues of  $\mathbf{F}$  to be non-negative, where  $\mathbf{F}$  is now the full 6 by 6 matrix:

$$\left. \begin{aligned} F_{11} + 2F_{12} \geq 0 \\ F_{11} - F_{12} \geq 0 \\ F_{44} \geq 0 \end{aligned} \right\} \Rightarrow \begin{cases} 3\sigma_s^2 \geq \sigma_t \sigma_c \\ -F_0 \geq 0 \end{cases} \quad (21)$$

leading to

$$\sigma_s \geq \frac{\sqrt{\sigma_t \sigma_c}}{\sqrt{3}} > \frac{\sqrt{\sigma_t \sigma_c}}{2}. \quad (22)$$

Note that the trivial conditions  $\sigma_s \geq 0$ ,  $\sigma_c \geq 0$ ,  $\sigma_t \geq 0$ ,  $F_0 \leq 0$  are already sufficient to ensure

$$F_{44} \geq 0, \quad F_{11} \geq 0, \quad F_{11} - F_{12} = 2F_{44} \geq 0. \quad (23)$$

And consequently, only the first eigenvalue may be negative. Note that the condition that the first eigenvalue must not be negative can be reformulated as  $F_{11} + 2F_{12} = -\frac{A_2}{9} \geq 0 \Rightarrow A_2 \leq 0$ .

In 3D principal stress space a convex quadratic yield surface corresponds to an ellipsoid, a cylinder or an ellipsoidal paraboloid. It should be noted here, that convexity in stress space is a sufficient condition for convexity in the invariant space spanned by the pressure and the vonMises stress but the reverse is not the case. Indeed consider the case of a linear relationship between the invariants (Drucker-Prager type law).

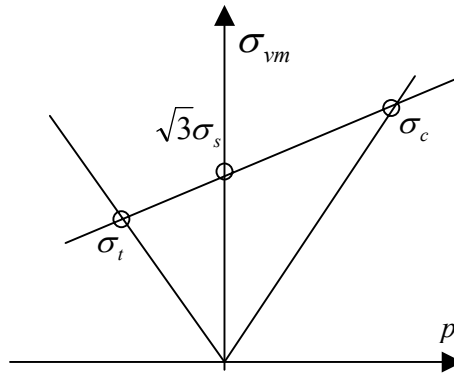


Figure 4: Drucker-Prager yield surface in invariant plane

This is a limiting case for convexity in the invariant plane and

$$\sqrt{3}\sigma_s = \frac{2\sigma_t\sigma_c}{\sigma_t + \sigma_c} \Rightarrow \sigma_s = \frac{\sqrt{\sigma_t\sigma_c} 2\sqrt{\sigma_t\sigma_c}}{\sqrt{3}(\sigma_t + \sigma_c)} \leq \frac{\sqrt{\sigma_t\sigma_c}}{\sqrt{3}} \quad (24)$$

Equation (24) shows that this yield surface is not convex in stress space if  $\sigma_c = \sigma_t$ . This corresponds to the vonMises cylinder. In general, a Drucker-Prager type law is represented by a cone in principal stress space. This surface is strictly spoken not convex because the cone consists of two blades. To complete our discussion a formal derivation of the convexity condition in the invariant plane is given by

$$\begin{aligned} f &= \sigma_{vm}^2 - A_0 - A_1 p - A_2 p^2 \\ \sigma_{vm} &= \sqrt{A_0 + A_1 p + A_2 p^2} \\ \frac{\partial^2 \sigma_{vm}}{\partial p^2} &\leq 0 \Rightarrow \sigma_s \geq \frac{2\sigma_t\sigma_c}{\sqrt{3}(\sigma_t + \sigma_c)} \end{aligned} \quad (25)$$

#### 2.1.2.4 Alternative formulation

Alternatively a yield surface containing a linear rather than a quadratic term was implemented in SAMP-1.

$$f = \sigma_{vm} - A_0 - A_1 p - A_2 p^2 \leq 0 \quad (26)$$

This formulation does not belong to the class of general quadratic yield surfaces that was just discussed. Coefficients are again easily identified from the uniaxial tension, compression and simple shear tests:

$$\left. \begin{aligned} \sigma_s \sqrt{3} &= A_0 \\ \sigma_t &= \sigma_s \sqrt{3} - A_1 \frac{\sigma_t}{3} + A_2 \frac{\sigma_t^2}{9} \\ \sigma_c &= \sigma_s \sqrt{3} + A_1 \frac{\sigma_c}{3} + A_2 \frac{\sigma_c^2}{9} \end{aligned} \right\} \Rightarrow \left\{ \begin{aligned} A_0 &= \sigma_s \sqrt{3} \\ A_1 &= 3 \left[ \frac{\sigma_t - \sigma_c}{\sigma_t + \sigma_c} - \sigma_s \sqrt{3} \frac{\sigma_t - \sigma_c}{\sigma_t \sigma_c} \right] \\ A_2 &= 18 \left[ \frac{1}{\sigma_t + \sigma_c} - \frac{\sigma_s \sqrt{3}}{2\sigma_t \sigma_c} \right] \end{aligned} \right. \quad (27)$$

This formulation may lead to some time savings if a vonMises or Drucker-Prager type yield surface is used (obtained respectively by simply setting  $A_1=A_2=0$  and  $A_2=0$ ). No full investigation concerning convexity was performed in this case and in general this formulation resulted in a more difficult fit to test results for different plastics. Convexity in invariant space requires that

$$A_2 \leq 0 \Rightarrow \sigma_s \sqrt{3} \geq \frac{2\sigma_t \sigma_c}{\sigma_c + \sigma_t} \quad (28)$$

## 2.2 Flow rule

Associated flow leads to the plastic strain rate in terms of the normal vector to the yield surface

$$\dot{\boldsymbol{\varepsilon}}_p = \dot{\lambda} \mathbf{n} = \dot{\lambda} \frac{\frac{\partial f}{\partial \boldsymbol{\sigma}}}{\left\| \frac{\partial f}{\partial \boldsymbol{\sigma}} \right\|} \quad \left\| \frac{\partial f}{\partial \boldsymbol{\sigma}} \right\| = \sqrt{\frac{\partial f}{\partial \boldsymbol{\sigma}} : \frac{\partial f}{\partial \boldsymbol{\sigma}}} \quad (29)$$

The volumetric plastic strain rate, deviatoric plastic strain rate and equivalent plastic strain rate are defined in the usual way:

$$\dot{\varepsilon}_{pv} = \text{tr}(\dot{\boldsymbol{\varepsilon}}_p) = \frac{\dot{\lambda}}{\left\| \frac{\partial f}{\partial \boldsymbol{\sigma}} \right\|} \text{tr} \left( \frac{\partial f}{\partial \boldsymbol{\sigma}} \right) \quad (30)$$

$$\begin{aligned} \dot{\boldsymbol{\varepsilon}}_{pd} &= \dot{\boldsymbol{\varepsilon}}_p - \frac{\dot{\varepsilon}_{pv}}{3} \boldsymbol{\delta} \\ \dot{\varepsilon}_p &= \sqrt{\frac{2}{3} \dot{\boldsymbol{\varepsilon}}_{pd} : \dot{\boldsymbol{\varepsilon}}_{pd}} = \frac{\dot{\lambda}}{\left\| \frac{\partial f}{\partial \boldsymbol{\sigma}} \right\|} \sqrt{\frac{2}{3} \left. \frac{\partial f}{\partial \boldsymbol{\sigma}} \right|_d : \left. \frac{\partial f}{\partial \boldsymbol{\sigma}} \right|_d} \end{aligned} \quad (31)$$

The associated flow for the general quadratic yield surface is defined as

$$\left. \begin{aligned} \frac{\partial \sigma_{vm}}{\partial \boldsymbol{\sigma}} &= \frac{3}{2\sigma_{vm}} \mathbf{s} \\ \frac{\partial p}{\partial \boldsymbol{\sigma}} &= -\frac{1}{3} \boldsymbol{\delta} \end{aligned} \right\} \Rightarrow \frac{\partial f}{\partial \boldsymbol{\sigma}} = 3\mathbf{s} + \frac{A_1 + 2A_2 p}{3} \boldsymbol{\delta} \quad (32)$$

$$\left\| \frac{\partial f}{\partial \boldsymbol{\sigma}} \right\| = \sqrt{9\mathbf{s} : \mathbf{s} + \frac{1}{3}(A_1 + 2A_2 p)^2} = \sqrt{6\sigma_{vm}^2 + \frac{1}{3}(A_1 + 2A_2 p)^2}$$

leading to the volumetric and deviatoric plastic strain rates respectively:

$$\begin{aligned} \dot{\varepsilon}_{vp} &= \dot{\lambda} (A_1 + 2A_2 p) / \left\| \frac{\partial f}{\partial \boldsymbol{\sigma}} \right\| \\ \dot{\boldsymbol{\varepsilon}}_{dp} &= \dot{\lambda} 3\mathbf{s} / \left\| \frac{\partial f}{\partial \boldsymbol{\sigma}} \right\| \end{aligned} \quad (33)$$

The equivalent plastic strain rate reads:

$$\begin{aligned}\dot{\varepsilon}_p &= \sqrt{\frac{2}{3} \dot{\boldsymbol{\varepsilon}}_{dp} : \dot{\boldsymbol{\varepsilon}}_{dp}} = \dot{\lambda} \sqrt{\frac{2}{3} 3\mathbf{s} : 3\mathbf{s}} / \left\| \frac{\partial f}{\partial \boldsymbol{\sigma}} \right\| \\ \dot{\varepsilon}_p &= \dot{\lambda} 2\sigma_{vm} / \left\| \frac{\partial f}{\partial \boldsymbol{\sigma}} \right\|\end{aligned}\quad (34)$$

It is instructive to derive the ratio of transversal to longitudinal plastic strain rate under uniaxial tensile and compressive loading. This ratio will here be called the “*plastic Poisson ratio*” although of course it is by no means a material constant:

$$\nu_p = -\frac{\dot{\varepsilon}_{yyp}}{\dot{\varepsilon}_{xyp}} = -\frac{\dot{\varepsilon}_{zyp}}{\dot{\varepsilon}_{xyp}} \quad (35)$$

It will be shown that additional restrictions are placed on the shape of the yield surface in order for the lateral behaviour of the material model to be reasonable under plastic loading. We therefore compute the plastic Poisson ratio in function of the yield surface:

$$\left. \begin{aligned}\dot{\varepsilon}_{vp} &= (1 - 2\nu_p) \dot{\varepsilon}_{xyp} \\ \dot{\varepsilon}_{xyp} &= \dot{\lambda} \left( 3s_{xx} + \frac{A_1 + 2A_2 p}{3} \right) / \|\mathbf{n}\| \\ \dot{\varepsilon}_{vp} &= \dot{\lambda} (A_1 + 2A_2 p) / \|\mathbf{n}\| \\ s_{xx} &= -2p\end{aligned}\right\} \Rightarrow A_1 + 2A_2 p = (1 - 2\nu_p) \left( -6p + \frac{A_1 + 2A_2 p}{3} \right) \quad (36)$$

This last expression yields

$$\nu_p = \frac{9 + 2A_2 + \frac{A_1}{p}}{18 - 2A_2 - \frac{A_1}{p}}, \quad (37)$$

and shows that the plastic Poisson ratio is dependent on the pressure and in particular that the lateral behaviour of the material is different in tension and in compression. This can be estimated further as:

$$\left\{ \begin{aligned}p < 0 &\Rightarrow p = -\frac{\sigma_t}{3} \Rightarrow \nu_p = \frac{9 + 2A_2 - \frac{3A_1}{\sigma_t}}{18 - 2A_2 + \frac{3A_1}{\sigma_t}} = \frac{\sigma_t^2}{\sigma_s^2} \frac{\sigma_c}{\sigma_t + \sigma_c} - 1 \\ p > 0 &\Rightarrow p = \frac{\sigma_c}{3} \Rightarrow \nu_p = \frac{9 + 2A_2 + \frac{3A_1}{\sigma_c}}{18 - 2A_2 - \frac{3A_1}{\sigma_c}} = \frac{\sigma_c^2}{\sigma_s^2} \frac{\sigma_t}{\sigma_t + \sigma_c} - 1\end{aligned}\right. \quad (38)$$

These equations can be solved for the shear yield:

$$\left\{ \begin{aligned}p < 0 &\Rightarrow \nu_p = \frac{\sigma_t^2}{\sigma_s^2} \frac{\sigma_c}{\sigma_t + \sigma_c} - 1 \Rightarrow \sigma_s^2 = \frac{\sigma_t^2}{1 + \nu_p} \frac{\sigma_c}{\sigma_t + \sigma_c} \\ p > 0 &\Rightarrow \nu_p = \frac{\sigma_c^2}{\sigma_s^2} \frac{\sigma_t}{\sigma_t + \sigma_c} - 1 \Rightarrow \sigma_s^2 = \frac{\sigma_c^2}{1 + \nu_p} \frac{\sigma_t}{\sigma_t + \sigma_c}\end{aligned}\right. \quad (39)$$

The latter shows that reasonable values for the plastic Poisson ratio put certain requirements on the yield surface:

$$0 \geq \nu_p \geq 0.5 \Rightarrow \begin{cases} p < 0 \Rightarrow \frac{\sigma_t \sigma_c}{3} \frac{2\sigma_t}{\sigma_t + \sigma_c} \leq \sigma_s^2 \leq \frac{\sigma_t \sigma_c}{3} \frac{3\sigma_t}{\sigma_t + \sigma_c} \\ p > 0 \Rightarrow \frac{\sigma_t \sigma_c}{3} \frac{2\sigma_c}{\sigma_t + \sigma_c} \leq \sigma_s^2 \leq \frac{\sigma_t \sigma_c}{3} \frac{3\sigma_c}{\sigma_t + \sigma_c} \end{cases} \quad (40)$$

Whereas convexity required only a lower limit for the shear yield, plausible plastic flow also imposes an upper limit with respect to tensile and compressive yield values. As it will be difficult in general to guarantee reasonable flow behaviour from three independent measurements in shear, tension and compression, a simplified flow rule has been implemented as the default in SAMP-1. The generally non-associated flow surface is given as

$$g = \sigma_{vm}^2 + \alpha p^2. \quad (41)$$

This flow rule is associated iff  $A_1 = 0$ ,  $A_2 = -\alpha$ . And clearly leads to a constant value for the plastic Poisson ratio

$$\nu_p = \frac{9 - 2\alpha}{18 + 2\alpha} \Rightarrow \alpha = \frac{9(1 - 2\nu_p)}{2(1 + \nu_p)}. \quad (42)$$

Plausible flow behaviour just means that  $0 \leq \alpha \leq \frac{9}{2} \Rightarrow 0 \leq \nu_p \leq 0.5$ . In SAMP-1 the value of the

plastic Poisson coefficient is given by the user, either as a constant or as a load curve in function of the uniaxial plastic strain. This allows to adjust the flow rule of the material to measurements of transversal deformation during uniaxial tensile or compressive testing. This can be important for plastics since often a non-isochoric behaviour is measured. The possible values for the plastic Poisson ratio and the resulting flow behaviour are sketched in Figure 5.

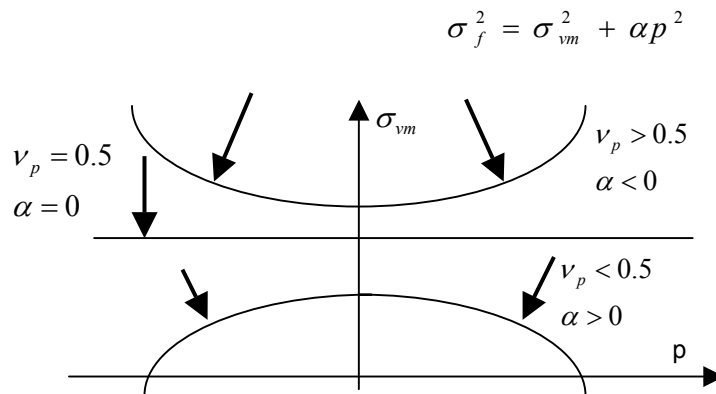


Figure 5: Influence of the flow rule on the plastic Poisson ratio

The volumetric and deviatoric plastic strain rates in this case are given as

$$\dot{\varepsilon}_{vp} = \dot{\lambda}(-2\alpha p) / \left\| \frac{\partial g}{\partial \sigma} \right\| = \frac{\dot{\lambda}(-2\alpha p)}{\sqrt{6\sigma_{vm}^2 + \frac{4}{3}\alpha^2 p^2}} \quad (43)$$

$$\dot{\varepsilon}_{dp} = \dot{\lambda}3s / \left\| \frac{\partial g}{\partial \sigma} \right\| = \frac{\dot{\lambda}3s}{\sqrt{6\sigma_{vm}^2 + \frac{4}{3}\alpha^2 p^2}}$$

In SAMP-1 the formulation is slightly modified and based on a flow rule

$$g' = \sqrt{\sigma_{vm}^2 + \alpha p^2} \quad (44)$$

The plastic strain rate computation is not normalized:

$$\dot{\varepsilon}_p = \dot{\lambda} \frac{\partial g'}{\partial \sigma} \quad (45)$$

The volumetric and deviatoric plastic strain rates in this case are given as:

$$\dot{\varepsilon}_{vp} = \dot{\lambda}(-2\alpha p) / 2g' = \frac{\dot{\lambda}(-2\alpha p)}{\sqrt{4\sigma_{vm}^2 + 4\alpha p^2}} \quad (46)$$

$$\dot{\varepsilon}_{dp} = \dot{\lambda}3s / 2g' = \frac{\dot{\lambda}3s}{\sqrt{4\sigma_{vm}^2 + 4\alpha p^2}}$$

This amounts to a different definition of the plastic consistency parameter  $\dot{\lambda}$  which of course has to be considered when equivalent plastic strain values are computed.

### 2.3 Hardening formulation

The hardening formulation is the attractive part of SAMP-1. The formulation is fully tabulated and consequently the user can directly input measurement results from uniaxial tension, uniaxial compression and simple shear tests in terms of load curves giving the yield stress as a function of the corresponding plastic strain. No fitting of coefficients is required. The test results that are reflected in the load curves will be used exactly by SAMP-1 without fitting to any analytical expression. Consequently the hardening will be dependent on the state of stress and not only on the plastic strain. The load curves that are expected as input are briefly described here:

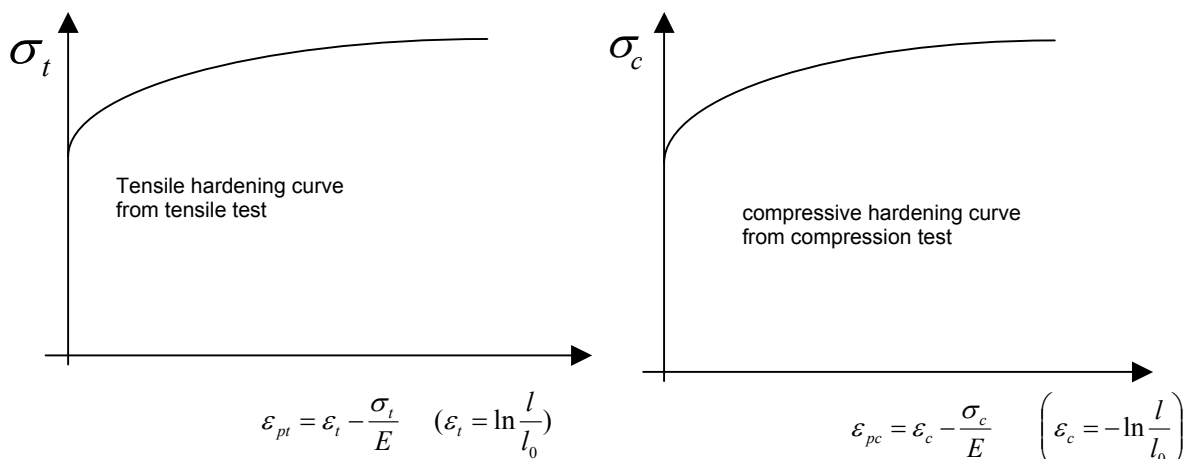


Figure 6: Hardening curve in tension and compression

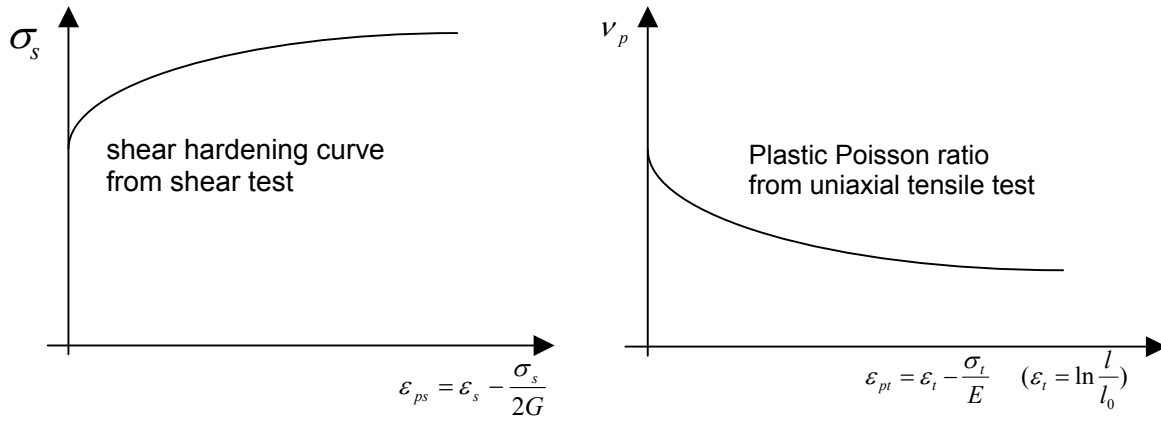


Figure 7: Hardening curve in shear and tabulated plastic Poisson ratio

The hardening rule now requires to define the evolution of all hardening parameters as a function of the plastic consistency parameter:

$$\dot{A}_0 = \frac{\partial A_0}{\partial \lambda} \dot{\lambda}, \quad \dot{A}_1 = \frac{\partial A_1}{\partial \lambda} \dot{\lambda}, \quad \dot{A}_2 = \frac{\partial A_2}{\partial \lambda} \dot{\lambda}, \quad \dot{\alpha} = \frac{\partial \alpha}{\partial \lambda} \dot{\lambda}. \quad (47)$$

The first three equations must be rewritten as follows:

$$\left. \begin{array}{l} A_0 = 3\sigma_s^2 \\ \frac{\partial A_0}{\partial \lambda} = \frac{\partial A_0}{\partial \sigma_s} \frac{\partial \sigma_s}{\partial \lambda} + \frac{\partial A_0}{\partial \sigma_t} \frac{\partial \sigma_t}{\partial \lambda} + \frac{\partial A_0}{\partial \sigma_c} \frac{\partial \sigma_c}{\partial \lambda} \end{array} \right\} \frac{\partial A_0}{\partial \lambda} = 6\sigma_s \frac{\partial \sigma_s}{\partial \lambda} \quad (48)$$

$$\left. \begin{array}{l} A_1 = 9\sigma_s^2 \frac{\sigma_c - \sigma_t}{\sigma_t \sigma_c} \\ \frac{\partial A_1}{\partial \lambda} = \frac{\partial A_1}{\partial \sigma_s} \frac{\partial \sigma_s}{\partial \lambda} + \frac{\partial A_1}{\partial \sigma_t} \frac{\partial \sigma_t}{\partial \lambda} + \frac{\partial A_1}{\partial \sigma_c} \frac{\partial \sigma_c}{\partial \lambda} \end{array} \right\} \frac{\partial A_1}{\partial \lambda} = 18\sigma_s \frac{\sigma_c - \sigma_t}{\sigma_t \sigma_c} \frac{\partial \sigma_s}{\partial \lambda} - 9 \frac{\sigma_s^2}{\sigma_t^2} \frac{\partial \sigma_t}{\partial \lambda} + 9 \frac{\sigma_s^2}{\sigma_c^2} \frac{\partial \sigma_c}{\partial \lambda} \quad (49)$$

$$\left. \begin{array}{l} A_2 = 9 \left( \frac{\sigma_t \sigma_c - 3\sigma_s^2}{\sigma_t \sigma_c} \right) \\ \frac{\partial A_2}{\partial \lambda} = \frac{\partial A_2}{\partial \sigma_s} \frac{\partial \sigma_s}{\partial \lambda} + \frac{\partial A_2}{\partial \sigma_t} \frac{\partial \sigma_t}{\partial \lambda} + \frac{\partial A_2}{\partial \sigma_c} \frac{\partial \sigma_c}{\partial \lambda} \end{array} \right\} \frac{\partial A_2}{\partial \lambda} = 9 \left( -\frac{6\sigma_s}{\sigma_t \sigma_c} \frac{\partial \sigma_s}{\partial \lambda} + \left( \frac{3\sigma_s^2}{\sigma_t^2 \sigma_c} \right) \frac{\partial \sigma_t}{\partial \lambda} + \left( \frac{3\sigma_s^2}{\sigma_t \sigma_c^2} \right) \frac{\partial \sigma_c}{\partial \lambda} \right) \quad (50)$$

The following conversion

$$\frac{\partial \sigma_s}{\partial \lambda} = \frac{\partial \sigma_s}{\partial \varepsilon_{ps}} \frac{\partial \varepsilon_{ps}}{\partial \lambda}, \quad \frac{\partial \sigma_t}{\partial \lambda} = \frac{\partial \sigma_t}{\partial \varepsilon_{pt}} \frac{\partial \varepsilon_{pt}}{\partial \lambda}, \quad \frac{\partial \sigma_c}{\partial \lambda} = \frac{\partial \sigma_c}{\partial \varepsilon_{pc}} \frac{\partial \varepsilon_{pc}}{\partial \lambda} \quad (51)$$

is defined to fully determine the hardening mechanism by performing three table lookups during every iteration in each time step. The table lookups give the yield stress and the tangent as a function of plastic strain for each experiment. From  $\lambda$  we obtain:

$$\varepsilon_{ps} \Rightarrow \sigma_s, \frac{\partial \sigma_s}{\partial \varepsilon_{ps}}, \quad \varepsilon_{pt} \Rightarrow \sigma_t, \frac{\partial \sigma_t}{\partial \varepsilon_{pt}}, \quad \varepsilon_{pc} \Rightarrow \sigma_c, \frac{\partial \sigma_c}{\partial \varepsilon_{pc}} \quad (52)$$

What remains to be done is to establish the relationship between the plastic consistency parameter and the plastic strains that were measured under uniaxial tension/compression and simple shear. To

achieve this, the equivalent plastic strain rate as a function of the plastic consistency parameter is generally used. Note that the hardening rule must be carefully considered at this point:

$$\dot{\boldsymbol{\varepsilon}}_p = \sqrt{\frac{2}{3} \dot{\boldsymbol{\varepsilon}}_{dp} : \dot{\boldsymbol{\varepsilon}}_{dp}}$$

<i>non – associated (default)</i>	<i>associated</i>	
$\dot{\boldsymbol{\varepsilon}}_p = \frac{\dot{\lambda}}{2g} \sqrt{\frac{2}{3} \frac{\partial \sigma_{vm}}{\partial \sigma} : \frac{\partial \sigma_{vm}}{\partial \sigma}}$	$\dot{\boldsymbol{\varepsilon}}_p = \frac{\dot{\lambda}}{\ \mathbf{n}\ } \sqrt{\frac{2}{3} \frac{\partial \sigma_{vm}}{\partial \sigma} : \frac{\partial \sigma_{vm}}{\partial \sigma}}$	(53)
$\dot{\boldsymbol{\varepsilon}}_p = \frac{\dot{\lambda}}{2g} \sqrt{\frac{2}{3} 3s:3s}$	$\dot{\boldsymbol{\varepsilon}}_p = \frac{\dot{\lambda}}{\ \mathbf{n}\ } \sqrt{\frac{2}{3} 3s:3s}$	
$\dot{\boldsymbol{\varepsilon}}_p = \dot{\lambda} \frac{\sigma_{vm}}{g}$	$\dot{\boldsymbol{\varepsilon}}_p = \dot{\lambda} \frac{2\sigma_{vm}}{\ \mathbf{n}\ }$	

Furthermore, the relationship between the individual plastic strain rate values and the consistency parameter is established. For the uniaxial case we get

$$\dot{\boldsymbol{\varepsilon}}_p = \begin{pmatrix} \dot{\varepsilon}_{pct} & 0 & 0 \\ 0 & -\nu_p \dot{\varepsilon}_{pct} & 0 \\ 0 & 0 & -\nu_p \dot{\varepsilon}_{pct} \end{pmatrix}$$

$$\dot{\boldsymbol{\varepsilon}}_p = \sqrt{\frac{2}{3} \dot{\boldsymbol{\varepsilon}}_{dp} : \dot{\boldsymbol{\varepsilon}}_{dp}} = |\dot{\varepsilon}_{pct}| \frac{2}{3} (1 + \nu_p)$$

$$|\dot{\varepsilon}_{pct}| = \dot{\varepsilon}_p \frac{3}{2(1 + \nu_p)} = \begin{cases} \dot{\lambda} \frac{\sigma_{vm}}{g} \frac{3}{2(1 + \nu_p)} \\ \dot{\lambda} \frac{2\sigma_{vm}}{\|\mathbf{n}\|} \frac{3}{2(1 + \nu_p)} \end{cases}$$

Similarly the plastic strain rate under shear loading is obtained by

$$\dot{\boldsymbol{\varepsilon}}_p = \dot{\boldsymbol{\varepsilon}}_{dp} = \begin{pmatrix} 0 & \dot{\varepsilon}_{ps} & 0 \\ \dot{\varepsilon}_{ps} & 0 & 0 \\ 0 & 0 & 0 \end{pmatrix}$$

$$\dot{\boldsymbol{\varepsilon}}_p = \sqrt{\frac{2}{3} \dot{\boldsymbol{\varepsilon}}_{dp} : \dot{\boldsymbol{\varepsilon}}_{dp}} = \frac{2}{\sqrt{3}} |\dot{\varepsilon}_{ps}|$$

$$|\dot{\varepsilon}_{ps}| = \dot{\varepsilon}_p \frac{\sqrt{3}}{2} = \begin{cases} \dot{\lambda} \frac{\sigma_{vm}}{g} \frac{\sqrt{3}}{2} = \dot{\lambda} \frac{\sqrt{3}}{2} \\ \dot{\lambda} \frac{2\sigma_{vm}}{\|\mathbf{n}\|} \frac{\sqrt{3}}{2} \end{cases}$$

These equations always allow determination of individual plastic strain values and thus the abscissa values for the table-lookup operations from the plastic consistency parameter.

$$|\dot{\varepsilon}_{pct}| = \dot{\varepsilon}_p \frac{3}{2(1+\nu_p)} = \begin{cases} \dot{\lambda} \frac{\sigma_{vm}}{g} \frac{3}{2(1+\nu_p)} \Rightarrow |\varepsilon_{pct}| = \int \frac{\sigma_{vm}}{g} \frac{3}{2(1+\nu_p)} d\lambda \\ \dot{\lambda} \frac{2\sigma_{vm}}{\|\mathbf{n}\|} \frac{3}{2(1+\nu_p)} \Rightarrow |\varepsilon_{pct}| = \int \frac{\sigma_{vm}}{\|\mathbf{n}\|} \frac{3}{(1+\nu_p)} d\lambda \end{cases} \quad (56)$$

$$|\dot{\varepsilon}_{ps}| = \dot{\varepsilon}_p \frac{\sqrt{3}}{2} = \begin{cases} \dot{\lambda} \frac{\sigma_{vm}}{g} \frac{\sqrt{3}}{2} = \dot{\lambda} \frac{\sqrt{3}}{2} \Rightarrow |\varepsilon_{ps}| = \lambda \frac{\sqrt{3}}{2} \\ \dot{\lambda} \frac{2\sigma_{vm}}{\|\mathbf{n}\|} \frac{\sqrt{3}}{2} \Rightarrow |\varepsilon_{ps}| = \int \frac{2\sigma_{vm}}{\|\mathbf{n}\|} \frac{\sqrt{3}}{2} d\lambda \end{cases} \quad (57)$$

In case of non-associated flow and a constant plastic Poisson ratio the integration is easily done analytically:

$$|\dot{\varepsilon}_{pct}| = \dot{\lambda} \frac{\sigma_{vm}}{g} \frac{3}{2(1+\nu_p)} \Rightarrow |\varepsilon_{pct}| = \lambda \sqrt{\frac{3}{2(1+\nu_p)}} \quad (58)$$

and

$$|\dot{\varepsilon}_{ps}| = \dot{\lambda} \frac{\sqrt{3}}{2} \Rightarrow |\varepsilon_{ps}| = \lambda \frac{\sqrt{3}}{2} \quad (59)$$

In this case the conversion of the tangent values that result from the table lookups is equally trivial:

$$\frac{\partial \sigma_s}{\partial \lambda} = \frac{\sqrt{3}}{2} \frac{\partial \sigma_s}{\partial \varepsilon_{ps}}, \quad \frac{\partial \sigma_t}{\partial \lambda} = \frac{\sqrt{3}}{\sqrt{2(1+\nu_p)}} \frac{\partial \sigma_t}{\partial \varepsilon_{pt}}, \quad \frac{\partial \sigma_c}{\partial \lambda} = \frac{\sqrt{3}}{\sqrt{2(1+\nu_p)}} \frac{\partial \sigma_c}{\partial \varepsilon_{pc}} \quad (60)$$

In the case of associated flow the conversion factors are not constants and must be evaluated at each time step

$$\begin{aligned} \frac{\partial \sigma_s}{\partial \lambda} &= \frac{\partial \sigma_s}{\partial \varepsilon_{ps}} \frac{\partial \varepsilon_{ps}}{\partial \lambda} \approx \frac{\partial \sigma_s}{\partial \varepsilon_{ps}} \frac{2\sigma_{vm}}{\|\mathbf{n}\|} \frac{\sqrt{3}}{2} \\ \frac{\partial \sigma_t}{\partial \lambda} &= \frac{\partial \sigma_t}{\partial \varepsilon_{pt}} \frac{\partial \varepsilon_{pt}}{\partial \lambda} \approx \frac{\partial \sigma_t}{\partial \varepsilon_{pt}} \frac{2\sigma_{vm}}{\|\mathbf{n}\|} \frac{3}{2(1+\nu_p)} \\ \frac{\partial \sigma_c}{\partial \lambda} &= \frac{\partial \sigma_c}{\partial \varepsilon_{pc}} \frac{\partial \varepsilon_{pc}}{\partial \lambda} \approx \frac{\partial \sigma_c}{\partial \varepsilon_{pc}} \frac{2\sigma_{vm}}{\|\mathbf{n}\|} \frac{3}{2(1+\nu_p)} \end{aligned} \quad (61)$$

## 2.4 Rate effects

Plastics are usually highly rate dependent. A proper visco-plastic consideration of the rate effects is therefore important in the numerical treatment of the material law. Data to determine the rate dependency are based on uniaxial dynamic testing. If dynamic tests are available, then the load curve defining the yield stress in uniaxial tension is simply replaced by a table definition. Similar to MAT\_24 this table contains multiple load curves corresponding to different values of the plastic strain rate as illustrated in Figure 8.

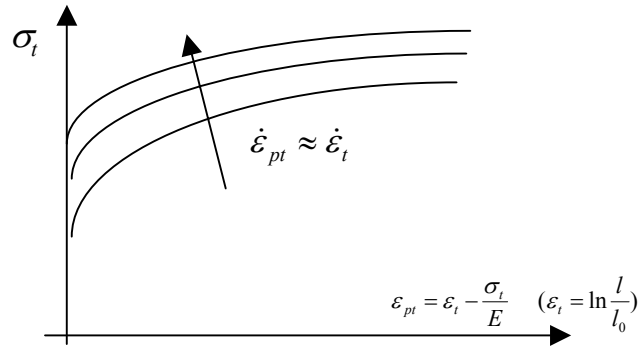


Figure 8: Tensile hardening curve from dynamic tensile tests

Subsequently table lookups involve determining static yield values for tension, compression and shear, as well as dynamic yield values in tension. Tangents with respect to the strain rate must also be evaluated:

$$\begin{aligned}
 \varepsilon_{ps} &\Rightarrow \sigma_{s0}, \left. \frac{\partial \sigma_s}{\partial \varepsilon_{ps}} \right|_0 \\
 \varepsilon_{pt}, \dot{\varepsilon}_{pt} = 0 &\Rightarrow \sigma_{t0}, \left. \frac{\partial \sigma_t}{\partial \varepsilon_{pt}} \right|_0 \\
 \varepsilon_{pt}, \dot{\varepsilon}_{pt} &\Rightarrow \sigma_t, \left. \frac{\partial \sigma_t}{\partial \varepsilon_{pt}} \right|_0, \left. \frac{\partial \sigma_t}{\partial \dot{\varepsilon}_{pt}} \right|_0 \\
 \varepsilon_{pc} &\Rightarrow \sigma_{c0}, \left. \frac{\partial \sigma_c}{\partial \varepsilon_{pc}} \right|_0
 \end{aligned} \tag{62}$$

Furthermore it is assumed that the rate effect in compression and shear is similar to the rate effect in tensile loading:

$$\sigma_s = \sigma_{s0} \frac{\sigma_t}{\sigma_{t0}}, \quad \sigma_c = \sigma_{c0} \frac{\sigma_t}{\sigma_{t0}} \tag{63}$$

These tangents to the yield surface are computed consistently with the previous assumption leading to

$$\begin{aligned}
 \left. \frac{\partial \sigma_s}{\partial \varepsilon_{ps}} \right|_0 &= \left. \frac{\partial \sigma_s}{\partial \varepsilon_{ps}} \right|_0 \left. \frac{\partial \sigma_{tc}}{\partial \varepsilon_{pt}} \left( \left. \frac{\partial \sigma_{tc}}{\partial \varepsilon_{pt}} \right|_0 \right)^{-1} \right. \\
 \left. \frac{\partial \sigma_c}{\partial \varepsilon_{pc}} \right|_0 &= \left. \frac{\partial \sigma_c}{\partial \varepsilon_{pc}} \right|_0 \left. \frac{\partial \sigma_{tc}}{\partial \varepsilon_{pt}} \left( \left. \frac{\partial \sigma_{tc}}{\partial \varepsilon_{pt}} \right|_0 \right)^{-1} \right. \\
 \frac{\partial \sigma_s}{\partial \dot{\varepsilon}_{ps}} &= \frac{\partial \sigma_t}{\partial \dot{\varepsilon}_{pt}} \frac{\sigma_{s0}}{\sigma_{t0}} \\
 \frac{\partial \sigma_c}{\partial \dot{\varepsilon}_{pc}} &= \frac{\partial \sigma_t}{\partial \dot{\varepsilon}_{pt}} \frac{\sigma_{c0}}{\sigma_{t0}}
 \end{aligned} \tag{64}$$

Although this approach is certainly questionable since rate effects may depend on the state of stress, it is justified by the fact that dynamic test results are not easily obtainable under shear and compres-

sion. A generalisation involving table-type definitions for all three types of experiments could be implemented straight forward if needed.

## 2.5 Damage and failure

Numerous damage models can be found in the literature. Probably the simplest concept is elastic damage where the damage parameter (usually written as  $d$ ) is a function of the elastic energy and effectively reduces the elastic modulae of the material. In the case of ductile damage,  $d$  is a function of plastic straining and affects the yield stress rather than the elastic modulae. This is equivalent to plastic softening. In more sophisticated damage models,  $d$  depends on both the plastic straining and the elastic energy (and maybe other factors) and affects yield stress as well as elastic modulae. (see [20]). A simple damage model was added to the SAMP-1 material law where the damage parameter  $d$  is a function of plastic strain only. A load curve must be provided by the user giving  $d$  as a function of the (true) plastic strain under uniaxial tension. The value of the critical damage  $D_c$  leading to rupture is then the only other required additional input. The implemented damage model is isotropic. Furthermore the model uses the notion of the effective cross section, which is the true cross section of the material minus the cracks that have developed. We define the effective stress as the force divided by the effective cross section

$$\sigma = \frac{f}{A}, \quad \sigma_{eff} = \frac{f}{A_{eff}} = \frac{f}{A(1-d)} = \frac{\sigma}{1-d}, \quad (65)$$

which allows to define an effective yield stress of

$$\sigma_{y,eff} = \frac{\sigma_y}{1-d}, \quad (66)$$

see [20]. By application of the principle of strain equivalence, stating that if the undamaged modulus is used, the effective stress corresponds to the same elastic strain as the true stress using the damaged modulus, one can write:

$$E = \frac{\sigma_{eff}}{\varepsilon_e}, \quad E_d = \frac{\sigma}{\varepsilon_e} = E(1-d) \quad (67)$$

Note that the plastic strains are therefore the same:

$$\varepsilon_p = \varepsilon - \frac{\sigma_{eff}}{E} = \varepsilon - \frac{\sigma}{E_d} \quad (68)$$

No damage will occur under pure elastic deformation with this model. The case of a material that is perfectly plastic in its undamaged state is illustrated in Figure 9.

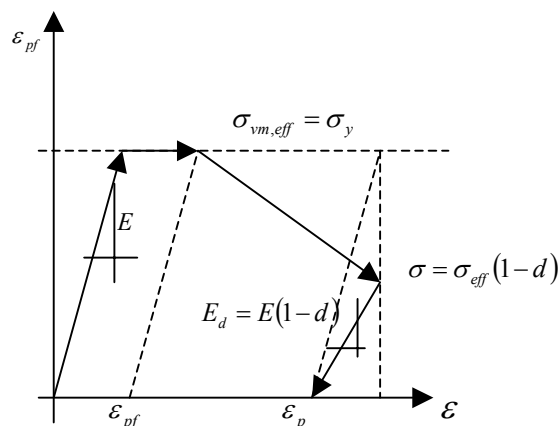


Figure 9: Damage formulation

It can be seen that the damage parameter effectively reduces the elastic modulus. Consequently if unloading is performed at different strain values during the uniaxial tensile test, the different unloading slopes allow to estimate the damage parameter for a given plastic strain:

$$d(\varepsilon_{pt}) = 1 - \frac{E_d(\varepsilon_{pt})}{E} \tag{69}$$

The damage model will thus be used essentially to fit the unloading behaviour of the material. The two stage process of determining input data from a measured true stress/strain curve is illustrated below. In a first step the damage curve is derived as given in Figure 10.

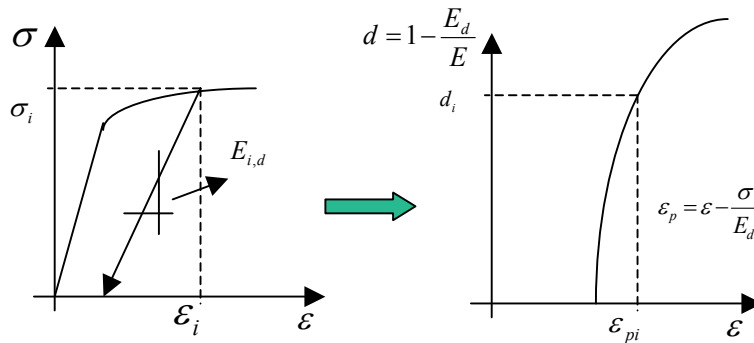


Figure 10: Determination of damage as a function of plastic strain

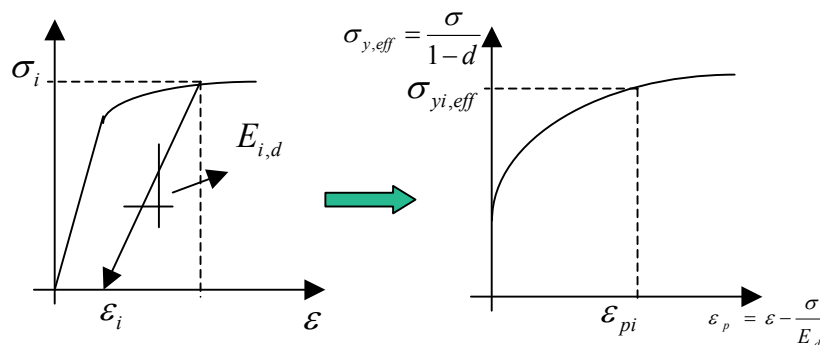


Figure 11: Conversion from true stress to effective hardening curve

And in a second step the hardening curve is determined in terms of effective stresses (see Figure 11). As usual the failure strain corresponds to the point where  $d=0$  and the rupture strain corresponds to the point where  $d$  reaches the critical value  $D_c$ .

If the damage curve is given a negative identification number in the LS-DYNA input, then the hardening curve data are expected in terms of true stresses and the input preparation is performed as if there were no damage (see Figure 12).

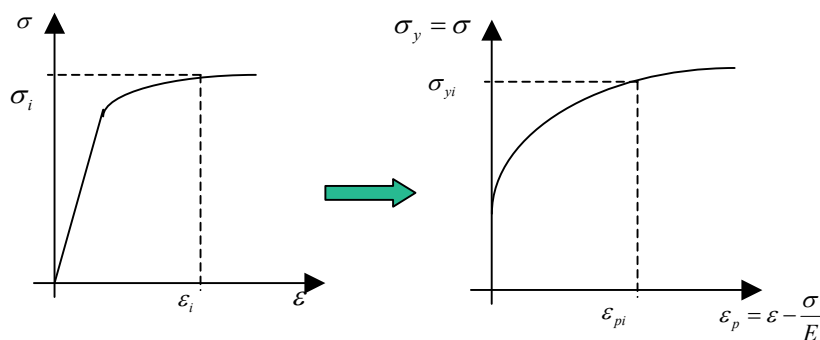


Figure 12: Conversion from true stress to hardening curve

In this case the numerically computed stress values will correspond to the input data and the damage model will seem to affect only the elastic modulae and thus the unloading/reloading behaviour of the material.

## 2.6 Crazing

Many plastics and PP-EPDM in particular show a localized deformation process called crazing. The material will typically change colour and turn white in the craze. From a mechanical point of view crazing can be identified with a permanent increase of volume (volumetric plastic straining) and a low biaxial strength. To simulate crazing it may therefore be desirable to consider biaxial test data in the numerical model. In SAMP-1 the hardening curve resulting from a biaxial tensile test is therefore optional as input. The curve should give yield stress as a function of volumetric strain and care must be taken to use the correct biaxial modulus when transforming from true strain to plastic strain. This is illustrated in Figure 13.

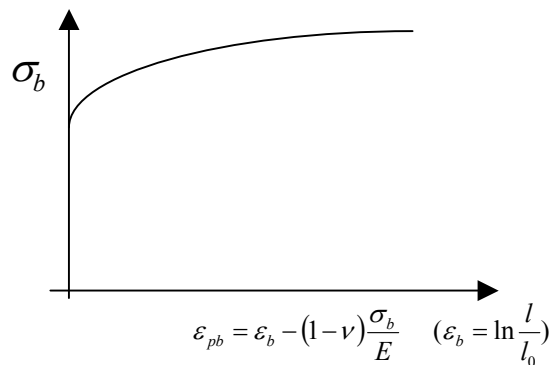


Figure 13: Biaxial hardening curve

In many practical cases where biaxial data are available, some other test result will be missing. In these cases the missing data is generated internally from the biaxial test result assuming a quadratic isotropic yield surface and the material law formulation is not changed.

## 2.7 Numerical implementation

### 2.7.1.1 Rate-independent plasticity iterations

To solve the equations of elasto-plasticity, the explicit cutting plane algorithm was selected. A complete review of the implementation is given below and is based on works of [16] and [17]. Consider the following set of equations defining the SAMP-1 material law:

$$\dot{\sigma} = 2G(\dot{\varepsilon}_d - \dot{\varepsilon}_d^p) + K(\dot{\varepsilon}_v - \dot{\varepsilon}_v^p)\delta \quad \text{material law}$$

$$\dot{q} = \begin{pmatrix} \dot{A}_0 \\ \dot{A}_1 \\ \dot{A}_2 \\ \dot{\alpha} \end{pmatrix} = \dot{\lambda} h = \dot{\lambda} \begin{pmatrix} \partial A_0 / \partial \lambda \\ \partial A_1 / \partial \lambda \\ \partial A_2 / \partial \lambda \\ \partial \alpha / \partial \lambda \end{pmatrix} \quad \text{hardening rule} \quad (70)$$

$$\dot{\varepsilon}^p = \dot{\lambda} r = \dot{\lambda} \frac{\partial g}{\partial \sigma} \quad \text{flow rule}$$

$$f = \begin{cases} \sigma_{vm}^2 - A_0 - A_1 p - A_2 p^2 \leq 0 & \text{iquad} = 1 \\ \sigma_{vm}^2 - A_0 - A_1 p - A_2 p^2 \leq 0 & \text{iquad} = 0 \end{cases} \quad \text{yield surface}$$

Here we can further specify the flow rule as follows:

$$\left. \begin{array}{l} iquad = 0/1 \\ \alpha \geq 0 \end{array} \right\} \Rightarrow \dot{\varepsilon}^p = \dot{\lambda} \mathbf{r} = \dot{\lambda} \frac{\partial \mathbf{g}}{\partial \boldsymbol{\sigma}} = \dot{\lambda} \frac{9s - 2\alpha p \delta}{6\sqrt{\sigma_{vm}^2 + \alpha p^2}}$$

$$\left. \begin{array}{l} iquad = 1 \\ \alpha > 0 \end{array} \right\} \Rightarrow \dot{\varepsilon}^p = \dot{\lambda} \mathbf{r} = \dot{\lambda} \frac{\partial \mathbf{g}}{\partial \boldsymbol{\sigma}} = \dot{\lambda} \frac{9s + (A_1 + A_2 p)\delta}{\sqrt{6\sigma_{vm}^2 + \frac{(A_1 + A_2 p)^2}{3}}} \quad (71)$$

It should be noted that no associated flow has been implemented for the alternative yield condition ( $iquad=0$ ).

#### 2.7.1.2 The damage model

The implementation of the damage model is trivially simple since the entire plasticity algorithm is performed in terms of effective stresses without any modification. In case the damage load curve has a negative identification number, the algorithm just amounts to modify the elastic modulus in each iteration:

$$E_{d,n}^k = E \left( 1 - d_n^k \left( \varepsilon_{pt,n}^k \right) \right) \quad (72)$$

#### 2.7.1.3 Rate effects

A constitutive law for visco-plastic materials is given for instance in [18] as:

$$\dot{\lambda} = \frac{\langle \Phi(f) \rangle}{\tau} \quad (73)$$

Here  $f$  is the yield function, so in our case  $f = \sigma_{vm}^2 - A_0 - A_1 p - A_2 p^2$ . The Föppl symbol (also known as McCauley-brackets) is used to indicate that the (visco-)plastic strain rates are zero as long as the state of stress is elastic. It should be emphasized at this point that the coefficients of the yield function  $f$  are not rate dependent.  $\Phi$  must be a dimensionless function and  $\tau$  is a relaxation time. In general  $\Phi$  need not be dimensionless and in [19] the visco-plastic constitutive law is given as

$$\dot{\varepsilon}_p = \frac{\langle \Phi(f) \rangle}{2\eta} \mathbf{r} \Rightarrow \dot{\lambda} = \frac{\langle \Phi(f) \rangle}{2\eta} \quad (74)$$

Here  $\eta$  has the dimension of a viscosity if  $\Phi$  has the dimension of a stress. This formulation is typically based on a constant viscosity and either a power law or exponential expression for  $\Phi$  and seems usually sufficient to describe the rate dependency of metals.

In the case of plastics, the rate dependency of the material is more pronounced and potentially has a different character. Therefore a tabulated formulation was chosen which gives the user full flexibility for fitting the model to test data. Uniaxial dynamic tensile tests allow tabulating the dynamic stress as a function of plastic strain and plastic strain rate. In the visco-plastic regime

$$2\eta\dot{\lambda} = \Phi(f) \Rightarrow f = \Phi^{-1}(2\eta\dot{\lambda}) \quad (75)$$

is obtained. Furthermore the constitutive equation is solved by

$$f(\lambda) - \Phi^{-1}(\dot{\lambda}) = 0 \quad (76)$$

This shows that the viscous overstress expressed by a positive value of the yield function  $f$  can be identified with the inverse function of  $\Phi$ . In contrast to the rate independent case now the constitutive law instead of the consistency equation is enforced. The cutting plane algorithm is applied accordingly.

### 3 Applications

#### 3.1 Yield surfaces of different thermoplastics

As a first example, the application of the present model due to prediction of yield for different thermoplastics is shown. The results are published in the thesis of Vogler [5]. For a review of methods commonly used in crash simulation, see [10], [11], [12] and the thesis of Koesters [4]. The results obtained by SAMP-1 are compared to the vonMises yield criterion. It must be emphasized that this criterion is usually used in crash simulation for modelling of thermoplastics. For a better understanding, the curves given in Figure 14 to Figure 16 are plotted in both the plane stress plane and the invariant plane, also known as p-q-plane or Burzynski-plane. The following experimental results are taken from Bardenheier [7].

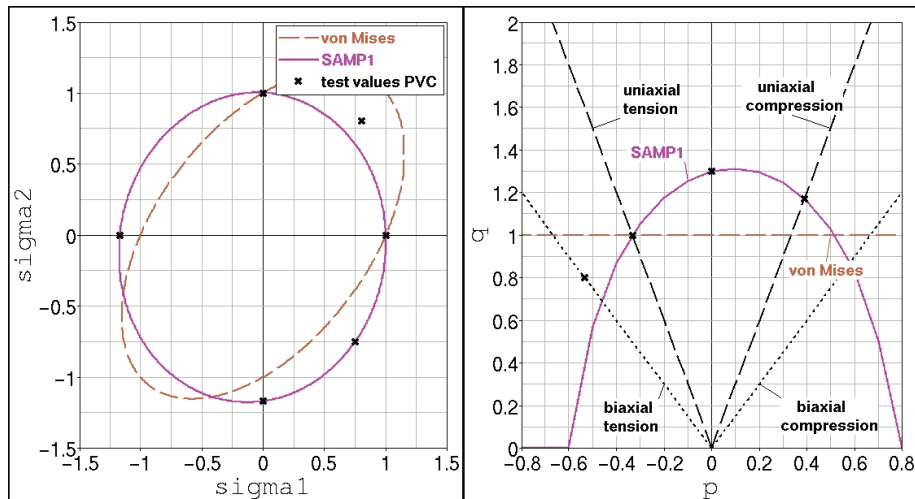


Figure 14: Yield surface of polyvinyl chloride (PVC)

In Figure 14, test data of polyvinyl chloride (PVC) is depicted. The dotted line represents results of the vonMises yield criterion and the solid line represents results obtained by SAMP-1. As can be seen, the vonMises yield surface is not capable to consider the different behaviour in compression, tension and shear. SAMP-1 yields to a much better agreement with the test. However, the experimental result under biaxial tension is not fitted exactly but approximated sufficiently. A method for further improvement of the result under biaxial tension is given by the least square fit which will be explained subsequently.

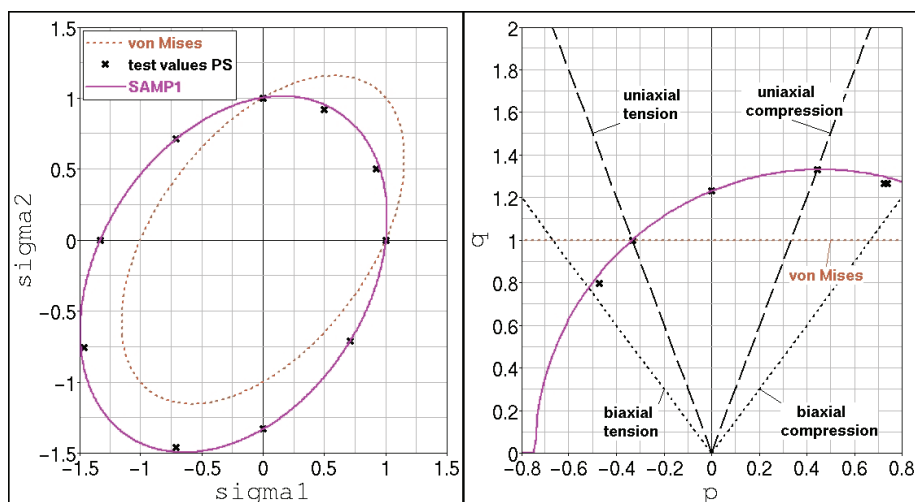


Figure 15: Yield surface of polystyrene (PS)

As a next example for a polymer that is widely used in engineering practice, polystyrene (PS) is regarded. For this polymeric material, more experimental results under different loading directions are available, see

Figure 15. Again, the vonMises criterion cannot describe the challenging material response. The results obtained by SAMP-1 are in good agreement with the experimental findings. This identifies the present model as an appropriate material law for polymers. Similar results can be observed for a polycarbonate (PC). Note that for polystyrene a convex yield surface is obtained in the p-q-plane. Three distinct points of the yield surface can be used directly to define the quadratic yield function in SAMP-1. In order to take four samples into account for the quadratic yield criterion, a least square approximation is applied. By such a numerical treatment, the experimental data under biaxial tension as well as test data of tension, compression and shear loading can be considered simultaneously.

In Figure 16, an acrylonitrile butadiene styrene (ABS) shows noticeable agreement. In the yield surface, this results in a softening behaviour under biaxial tension. As can be seen, using compression, tension and shear only, the yield behaviour cannot be described sufficiently by the SAMP-1 criterion. If biaxial tension is considered additionally by a least square fit, the (still convex) yield surface is much closer to the experimental data.

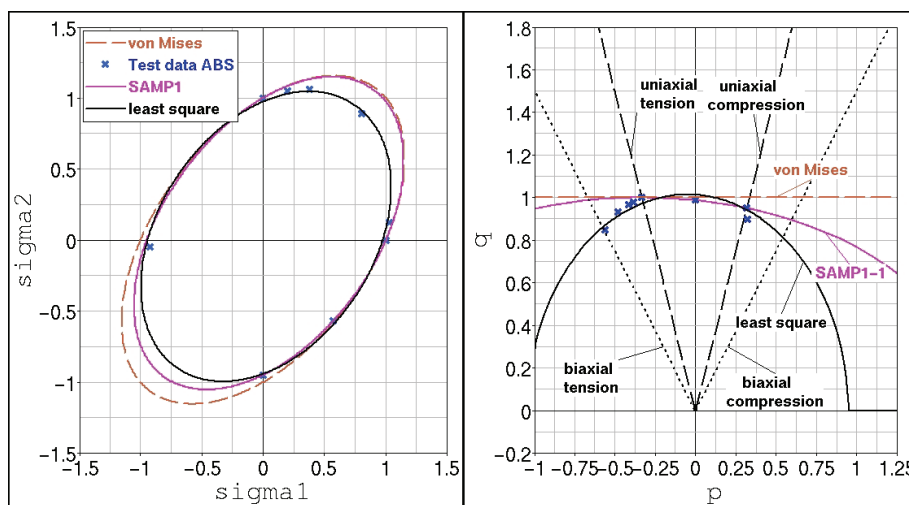


Figure 16: Yield surface of acrylonitrile butadiene styrene (ABS)

### 3.2 Verification and validation of PP-EPDM

#### 3.2.1 Dynamic tensile tests

The strain rate dependency of SAMP-1 is investigated by the simulation of dynamic tensile tests. The experimental setup consists of a bone shaped specimen with a total length of 48.6mm, see Figure 17. The area of uniaxial stress (8x20mm) is highlighted in the picture. All experiments have been performed, again, by [23].

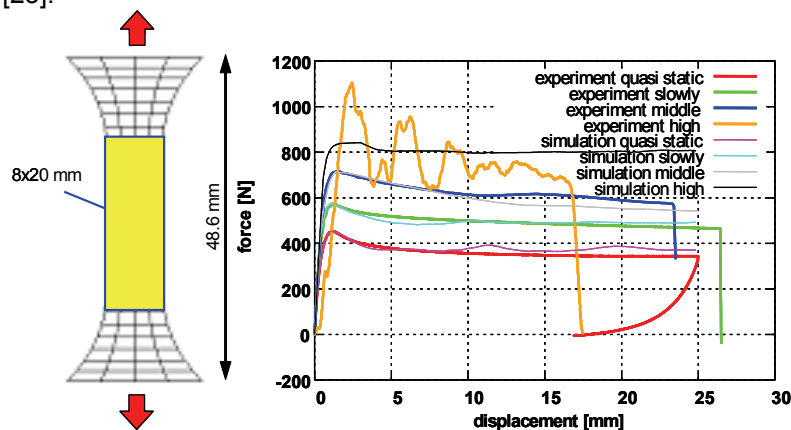


Figure 17: Dynamic tensile tests at different strain rates

The test data is input in the material card by defining tabulated local stress-strain curves measured at different strain rate levels. The bone shaped specimen is discretized with an element size that is typically used in crashsimulation. The choice of the same element size is necessary because of the well known strong mesh dependency due to strain-softening. An extension that applies to various element sizes is described in Feucht [24]. The global force and displacement are compared to the experimental response. The results are given in Figure 17. At this point, it has to be emphasized again that in SAMP-1 a real visco-plastic formulation is implemented, i.e. relaxation effects are taken into account as it is known from MAT\_PIECEWISE\_LINEAR\_PLASTICITY with VP=1.

### 3.2.2 Quasi-static tensile tests with unloading

In the numerical simulation of thermoplastics, the prediction of the elastic rebound of structures is an important issue, especially for pedestrian protection. The unloading behaviour is dominated by visco-elastic effects, i.e. viscosity below permanent deformation. However, visco-elasticity is not considered within SAMP-1 so far. Nevertheless, unloading can be approximated linearly by elastic damage, see [10], [11], and [12] for details. For parameter identification, unloading tests at different strain levels were performed by the [23]. The unloading path can then be approximated by the damage parameter  $d = d(\varepsilon_p)$  which acts on the effective Young's modulus.

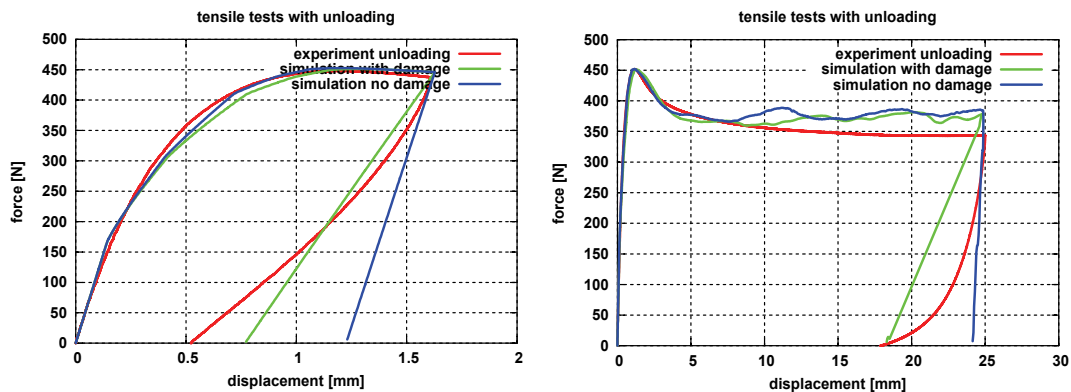


Figure 18: Tensile tests with unloading at different strain levels

In SAMP-1, this damage function can be tabulated in a load curve. Since the damage model of [20] is used, the yield function  $\sigma_y(\varepsilon_p)$  is affected by damage, too. That is, softening of the stress-strain curve may be expected. Usually, if elastic damage is to be taken into account only, the yield stress has to be modified according to  $\sigma_y \mapsto \sigma_y / (1 - d)$  as it is known from MAT\_PLASTICITY\_WITH\_DAMAGE (material no. 81) in LS-DYNA. To avoid such a cumbersome procedure, an additional feature has been implemented. If LCID-d is negative in the input, the modification of the yield stress is realized internally and the original stress-strain curve is reflected. The simulation results of a simple tensile test in comparison with experimental results are depicted in Figure 18. As can be seen, the reduction of the elastic parameters for increasing plastic strains considers the unloading behaviour approximately and the experimental stress-strain curve is recovered.

### 3.2.3 Compression test

The different behaviour of thermoplastics in compression and tension does not comply with a von-Mises type of plasticity as it is used in MAT\_PIECEWISE\_LINEAR\_PLASTICITY. In SAMP-1, the direct input of experimental data obtained from compression tests allows a straight forward treatment of the problem. In Figure 19, a draft of the experimental setup consisting of a bone shape specimen with a total length of 176.33mm is given. The area (40x60mm) of uniaxial stress is highlighted and, additionally, the dogbone specimen is supported perpendicular to the drawing plane to avoid local buckling. The specimen is again discretized with an element size used in full car models and the material properties are validated subsequently. The global force and displacement are compared to the measured response. The results given in Figure 19 show a good agreement. Note that the local stress-strain curve obtained in the experiment is simply used in the material card for the LCID-c. However, a pure uniaxial stress state is hard to achieve in both experiment and simulation. A certain interaction

with tension and shear cannot be avoided completely. This is even more pronounced in the shear test of the next example.

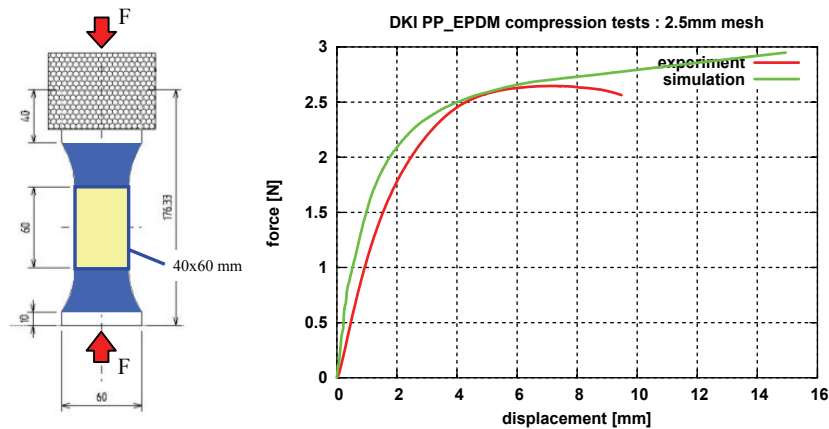


Figure 19: Compression test

### 3.2.4 Shear test

In Figure 20, a shear test has been simulated by using SAMP-1. Although a pure shear stress is certainly not given, the test can be simulated at least up to yield in a satisfactory way. For larger displacements, the model acts too stiff due to the large element size. Clearly, a further refinement is not advisable with regard to the time step size in a full car model. The effect is getting less pronounced for a finer mesh, though.

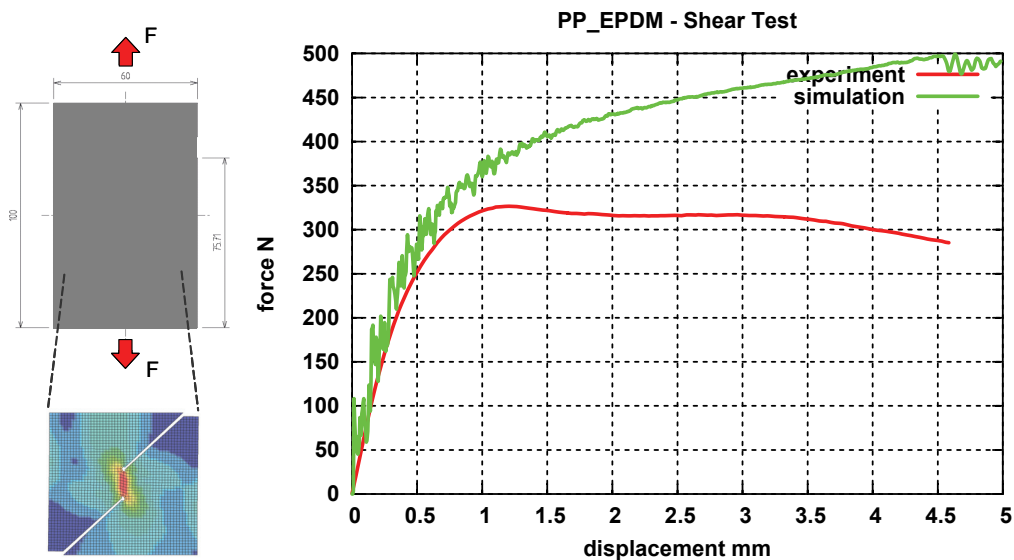


Figure 20: Shear test

### 3.2.5 Bending test

In Figure 21, the reaction force versus the displacement of a quasi-static three point bending test is shown. Because of the higher yield stress under compression, it is not possible to simulate the bending test by using a vonMises criterion solely based on the tensile test data. With SAMP-1, where the higher yield stress taken from the experiment under compression is considered, the bending test can be simulated with good agreement.

In conclusion it can be said that all the effects associated with thermoplastics given in the examples can be approximately considered in the present material model: necking and strain rate effects by

visco-plasticity, unloading behaviour by a (1-d)-damage model, different behaviour under compression and tension and thus a correct bending stiffness by the chosen yield surface.

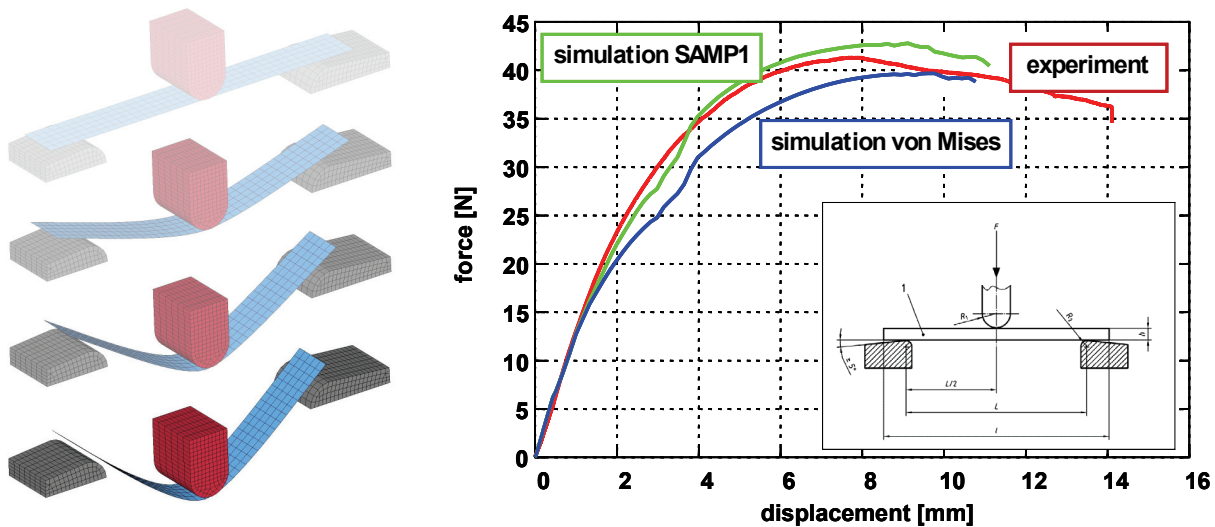


Figure 21: Three-point-bending test

#### 4 Conclusion and outlook

As an ever increasing percentage of the weight of an automobile is made out of plastic parts and these parts are safety-relevant, the industrial need for a reliable simulation tool can no longer be ignored. Such a tool is subject to the many constraints imposed by the context of an industrial development process: One has to balance the need for accuracy and respect for the actual physics with easiness of use, robustness and efficiency. For SAMP-1, we have therefore chosen a theoretical and numerical framework that is familiar, yet reasonably general. The result is, like any numerical methodology, a compromise.

As limitations of the current implementation we can cite the following:

- The method is completely phenomenological: No micromechanics are considered and no attempt is made to take the actual physical deformation processes of the plastic into account.
- The data input is based on test results that are partly difficult to obtain. The latter is primarily true for shear and biaxial loading but also for compressive loads and for any dynamic load involving stress relaxation processes.
- The application is limited to ductile plastics that are initially isotropic and remain isotropic throughout the deformation process. This will not be the case for most polymeric materials.
- In many cases the test data is hard to fit with a quadratic yield surface or will lead to a concave yield surface. Moreover, non-convex yield surfaces potentially generate problems in the numerical algorithm since a unique solution is no longer guaranteed. This situation can be countered balanced partly by assuming isochoric behaviour.

As positive aspects we shall mention:

- For many plastics we were able to obtain a reasonable fit of the experimental data; even if its rate dependency is high.
- The material law is equipped with special-purpose options to obtain a numerically robust response.
- The tabulated input will be transparent to most users.
- The setup of the user-subroutine is such that future extensions are easily incorporated.

Future work will focus on the load-induced anisotropy which develops naturally in plastics and on the implementation of more advanced damage and failure models. On the somewhat longer term, a visco-elasto-visco-plastic approach is envisioned to accommodate rate effects in the elastic region. Combined with the anisotropic formulation this can result in a model suiting also fibre reinforced components. Furthermore, the model is not restricted to thermoplastics, it should be emphasized that the

model is also capable to describe phenomenological the behaviour of structural foams and adhesives. And, of course, it includes metallic materials like steels and aluminium as a special case.

## 5 Literature

- [1] J.O. Hallquist: LS-DYNA, Theoretical Manual, Livermore Software Technology Corporation, Report 1018, 1991.
- [2] P.A. Du Bois: Crashworthiness Engineering Course Notes, Livermore Software Technology Corporation, 2004.
- [3] S. Kolling & A. Haufe: A constitutive model for thermoplastic materials subjected to high strain rates, Proceedings in Applied Mathematics and Mechanics • PAMM, submitted.
- [4] M. Koesters: Materialmodellierung von Thermoplasten mit Anwendungen in der Crashesimulation, Diplomarbeit DaimlerChrysler, 2004.
- [5] M. Vogler: Implementierung von visko-plastischen Stoffgesetzen für Thermoplaste, Diplomarbeit DaimlerChrysler, 2005.
- [6] T. Frank, A. Kurz, M. Pitzer & M. Soellner: Development and validation of numerical pedestrian impactor models. 4th European LS-DYNA Users Conference, pp. C-II-01/18, 2003.
- [7] R. Bardenheier: Mechanisches Versagen von Polymerwerkstoffen. Hanser-Verlag, 1982.
- [8] D.C. Drucker, W. Prager: Soil mechanics and plastic analysis or limit design. Quarterly of Applied Mathematics, 10:157-165, 1952.
- [9] D.C. Drucker: A definition of stable inelastic material. Journal of Applied Mechanics, 26:101-106, 1959.
- [10] P.A. Du Bois, S. Kolling, M. Koesters & T. Frank: Material modeling of polymeric materials in crashworthiness analysis. 3rd Workshop for Material and Structural Behaviour at Crash Processes (crashMAT), Freiburg, Germany 2004.
- [11] P. A. Du Bois, S. Kolling, M. Koesters & T. Frank: Material behaviour of polymers under impact loading. International journal of impact mechanics, 2005, in press.
- [12] P.A. Du Bois, M. Koesters, T. Frank & S. Kolling: Crashworthiness analysis of structures made from polymers. 3rd LS-DYNA Forum, Bamberg, Germany 2004. Conference Proceedings, ISBN 3-9809901-0-9, pp. C-I-01/12.
- [13] A. Haufe, P.A. Du Bois, S. Kolling & M. Feucht: A semi-analytical model for polymers subjected to high strain rates. 5th European LS-DYNA Users' Conference, Birmingham, England, 2005, Conference Proceedings, ARUP UK, pp. 2b-58.
- [14] A. Haufe, P.A. Du Bois, S. Kolling & M. Feucht: On the development, verification and validation of a semi-analytical model for polymers subjected to dynamic loading. International Conference on Adaptive Modeling and Simulation, ADMOS, Barcelona, Spain, 2005, Conference Proceedings.
- [15] M. Junginger: Charakterisierung und Modellierung unverstärkter thermoplastischer Kunststoffe zur numerischen Simulation von Crashvorgängen", Dissertation, Fraunhofer Gesellschaft, Germany, ISBN 3-8167-6339-1.
- [16] J.C. Simo, T.J.-R. Hughes: Elastoplasticity and viscoplasticity – computational aspects. Springer Series in Applied Mathematics, Springer, Berlin, 1989.
- [17] T.J.-R. Hughes: Numerical implementation of constitutive models: rate-independent deviatoric plasticity. In Nemat-Nasser et al: Theoretical foundation for large scale computations for nonlinear material behaviour. Martinus Nijhoff Publishers, Dordrecht, 1984.
- [18] T.J.-R. Hughes: Efficient and simple algorithms for the integration of general classes of inelastic constitutive equations including damage and rate effects. In T.J.-R. Hughes, T. Belytschko: nonlinear finite element analysis course notes, 2003.
- [19] P. Wriggers: Nichtlineare Finite-Element-Methoden, Springer-Verlag, 2001.
- [20] J. Lemaitre, J.-L. Chaboche: Mécanique des matériaux solides, Dunod, 1988.
- [21] W.W. Feng, W.H. Yang: general and specific quadratic yield functions, composites technology review.
- [22] V. Kolupaev, M. Moneke, N. Darsow: Modelling of the three-dimensional creep behaviour of non-reinforced thermoplastics, Computational Materials Science 32 (3-4) (2005), 400-406.
- [23] T. Gerster, M. Neumann: Dynamische Charakterisierung und Modellierung von vier Polymerwerkstoffen. Ernst-Mach-Institut für Kurzzeitdynamik (Interner Bericht), Freiburg/Germany, 2004
- [24] M. Feucht, W. Fassnacht: Simulation der duktilen Rissbildung in Crashberechnungen mit Hilfe des Gurson-Modells, 17. CADFEM User's meeting, Sonthofen/Germany, 1999.